MATERIALS SCIENCE / МАТЕРИАЛОВЕДЕНИЕ

UDC 538.953
DOI 10.17073/0368-0797-2024-4-440-448

Original article
Оригинальная статья

Molecular dynamics study of the influence of carbon impurity on austenite nanoparticles crystallization during rapid cooling

I. V. Zorya[1], G. M. Poletaev[2, 3], Yu. V. Bebikhov[4], A. S. Semenov[4]

[1] **Siberian State Industrial University** (42 Kirova Str., Novokuznetsk, Kemerovo Region – Kuzbass 654007, Russian Federation)
[2] **Katanov Khakassian State University** (90 Lenina Ave., Abakan, Republic of Khakassia 655012, Russian Federation)
[3] **Polzunov Altai State Technical University** (46 Lenina Ave., Barnaul, Altai Territory 656038, Russian Federation)
[4] **Mirny Polytechnic Institute (branch) of North-Eastern Federal University** (5 Tikhonova Str., Mirny, Republic of Sakha (Yakutia) 678170, Russian Federation)

zorya.i@mail.ru

Abstract. The molecular dynamics method was used to study the structure formation during austenite nanoparticles crystallization in the presence of carbon impurities. The paper describes the dependence of the melt cooling rate, particle size, concentration of carbon atoms in the particle on the resulting structure features during crystallization and temperature of the crystallization onset. Formation of the nanocrystalline structure of nanoparticles can be controlled by varying the cooling rate and introducing a carbon impurity: at a cooling rate above 10^{13} K/s in the model used, crystallization did not have time to occur; at a rate below $5 \cdot 10^{12}$ K/s, the austenite particle crystallized to form a nanocrystalline structure. At the same time, with a decrease in the cooling rate, a decrease in the density of defects in the final structure was observed. At a rate of $5 \cdot 10^{11}$ K/s or less, crystallization of carbon-free particles took place with the formation of low-energy grain boundaries (with a high density of conjugate nodes: special boundaries, twins). The crystallization temperature during cooling at a rate below 10^{12} K/s is inversely proportional to the particle diameter: as the particle size decreases, the proportion of free surface increases, which leads to a decrease in the probability of crystalline nuclei formation. In addition, the crystallization temperature increases with a decrease in the cooling rate. The introduction of a carbon impurity led to a decrease in the crystallization temperature of nanoparticles: in the presence of 10 at. %. As a percentage of carbon, it decreased by about 200 K for particles of different sizes. Carbon atoms often formed clusters consisting of several carbon atoms. Such clusters distorted the resulting crystal lattice of metal around them, preventing crystallization. In the presence of a carbon impurity, the final structure of the crystallized particles contained a higher density of grain boundaries and other defects. Carbon atoms, especially clusters of them, were fixed mainly at grain boundaries and triple joints.

Keywords: molecular dynamics, nanoparticle, crystallization, nanocrystal, austenite

Acknowledgements: The research was supported by the Russian Science Foundation (grant No. 23-12-20003, https://rscf.ru/project/23-12-20003/) and the Government of the Republic of Khakassia.

For citation: Zorya I.V., Poletaev G.M., Bebikhov Yu.V., Semenov A.S. Molecular dynamics study of the influence of carbon impurity on austenite nanoparticles crystallization during rapid cooling. *Izvestiya. Ferrous Metallurgy*. 2024;67(4):440–448.
https://doi.org/10.17073/0368-0797-2024-4-440-448

Молекулярно-динамическое исследование влияния примеси углерода на процесс кристаллизации наночастиц аустенита при быстром охлаждении

И. В. Зоря[1], Г. М. Полетаев[2, 3], Ю. В. Бебихов[4], А. С. Семенов[4]

[1] **Сибирский государственный индустриальный университет** (Россия, 654007, Кемеровская обл. – Кузбасс, Новокузнецк, ул. Кирова, 42)
[2] **Хакасский государственный университет им. Н.Ф. Катанова** (Россия, 655012, Республика Хакасия, Абакан, пр. Ленина, 90)
[3] **Алтайский государственный технический университет им. И.И. Ползунова** (Россия, 656038, Алтайский край, Барнаул, пр. Ленина, 46)
[4] **Политехнический институт Северо-Восточного федерального университета им. М.К. Аммосова** (Россия, 678170, Республика Саха (Якутия), Мирный, ул. Тихонова, 5)

zorya.i@mail.ru

Аннотация. Методом молекулярной динамики проведено исследование формирования структуры при кристаллизации наночастиц аустенита в условиях наличия примеси углерода. Рассматривалось влияние скорости охлаждения расплава, размера частиц, концентрации атомов углерода в частице на особенности образующейся структуры при кристаллизации и температуру начала кристаллизации. Показано, что формированием нанокристаллической структуры наночастиц можно управлять путем варьирования скорости охлаждения и введения примеси углерода: при скорости охлаждения выше 10^{13} К/с в используемой модели кристаллизация не успевала произойти, при скорости ниже $5 \cdot 10^{12}$ К/с частица аустенита кристаллизовалась с образованием нанокристаллической структуры. При этом при снижении скорости охлаждения наблюдалось уменьшение плотности дефектов в конечной структуре. При скорости $5 \cdot 10^{11}$ К/с и менее кристаллизация частиц без углерода проходила с образованием низкоэнергетических границ зерен (с высокой плотностью сопряженных узлов: специальных границ, двойников). Температура кристаллизации при охлаждении со скоростью ниже 10^{12} К/с обратно пропорциональна диаметру частицы: по мере уменьшения размера частицы увеличивается доля свободной поверхности, что приводит к уменьшению вероятности образования кристаллических зародышей. Кроме того, температура кристаллизации увеличивается при уменьшении скорости охлаждения. Введение примеси углерода приводило к снижению температуры кристаллизации наночастиц: при наличии 10 ат. % углерода она уменьшалась примерно на 200 К для частиц разного размера. Атомы углерода часто образовывали скопления, состоящие из нескольких атомов углерода. Такие скопления искажали образующуюся кристаллическую решетку металла вокруг себя, препятствуя кристаллизации. В условиях наличия примеси углерода конечная структура кристаллизовавшихся частиц имела более высокую плотность границ зерен и других дефектов. Атомы углерода, особенно скопления из них, закреплялись преимущественно на границах зерен и тройных стыках.

Ключевые слова: молекулярная динамика, наночастица, кристаллизация, нанокристалл, аустенит

Благодарности: Исследование выполнено за счет гранта Российского научного фонда (проект № 23-12-20003, https://rscf.ru/project/23-12-20003/) при паритетной финансовой поддержке Правительства Республики Хакасия.

Для цитирования: Зоря И.В., Полетаев Г.М., Бебихов Ю.В., Семенов А.С. Молекулярно-динамическое исследование влияния примеси углерода на процесс кристаллизации наночастиц аустенита при быстром охлаждении. *Известия вузов. Черная металлургия*. 2024;67(4):440–448. https://doi.org/10.17073/0368-0797-2024-4-440-448

Introduction

Metallic nanoparticles exhibit a unique set of physical, chemical, and optical properties. These properties make nanoparticles highly promising for applications in areas such as microelectronics, optoelectronics, plasmonics [1; 2], medicine and biology [3; 4], chemical catalysis, and the production of gas sensors [5; 6]. In the manufacturing of nanoparticles, significant attention is given to controlling the phase state, size, and shape of the particles due to their critical impact on beneficial properties [7 – 10]. Consequently, investigating the factors influencing the mechanisms and kinetics of phase transitions, as well as the final structure of the particles, is of great importance. Recently, particles with a high level of atomic structure disorder, such as amorphous or nanocrystalline structures, have garnered significant interest [11 – 14]. These particles possess high stored energy and a unique electronic structure, making them promising for use in catalysis, biomedicine, optics, and electronics [15 – 17].

A nanocrystalline structure, which is a polycrystalline structure with relatively small grain sizes (ranging from a few nanometers to several tens of nanometers) and a high density of non-equilibrium grain boundaries, can be obtained not only through intense deformation but also through sufficiently rapid cooling, where the recrystallization process is suppressed during grain growth, leading to the formation of numerous small grains [18; 19]. Through computer modeling in studies [20 – 23], it has been shown, for example, that nanoparticles of pure metals crystallize with a nanocrystalline structure with high grain boundary density and an average grain size of only

a few nanometers when cooled at a rate of approximately 10^{12} K/s from the molten state. In studies [20; 22; 23], it was demonstrated that at a cooling rate exceeding 10^{13} K/s, homogeneous crystallization does not have time to occur, and the cooled particles in the molecular dynamics model exhibit an amorphous structure.

The interaction of impurity atoms of light elements with metals is of significant scientific and technological interest. Even at low concentrations, atoms of carbon, nitrogen, and oxygen significantly affect the properties of metals. Despite the importance of understanding the mechanisms and processes underlying the influence of alloying with light element impurities on the properties of metals, many questions regarding the behavior of impurities at the atomic level in the metallic matrix remain unresolved. One such question is the determination of the impact of impurities on phase transitions, particularly the exploration of ways to control the temperature intervals of phase existence in metallic nanomaterials by varying impurities. This study is devoted to investigating, at the atomic level using molecular dynamics, the crystallization process of austenite nanoparticles and the effect of carbon impurity on these processes.

Model description

For describing Fe–Fe interactions in austenite, the Lau EAM potential [24] was used, which accurately reproduces the structural, energetic, and elastic characteristics of austenite [24; 25]. To describe the interactions of iron atoms with carbon atoms and carbon atoms with each other in the metal matrix, Morse potentials [26] were used, determined based on experimental data on the dissolution energy and migration energy of carbon impurity atoms in the austenite crystal, atomic radii, their electronegativity, binding energy, and other characteristics.

In the model, a spherical austenite particle was initially created by cutting out a sphere of the appropriate size from an ideal FCC crystal. Particles with diameters ranging from 1.5 to 12.0 nm were considered. The particle was placed in a rectangular parallelepiped calculation cell with periodic boundary conditions. Although free conditions (i.e., the absence of any boundary conditions) can be used for this model, periodic boundary conditions were employed in this study to ensure that atoms evaporating from the particle surface at high temperatures do not escape far from the particle but remain within the calculation cell. The distance between the walls of the calculation cell was sufficiently large to prevent interaction between the particle and its virtual duplicate [27; 28].

Carbon impurity atoms were introduced randomly throughout the entire volume of the metallic particle. The impurity concentration varied from 0 to 10 at. %. After creating the initial spherical particle, structural relaxation was performed to establish the equilibrium atomic structure. Temperature control was carried out using the Nose-Hoover thermostat. The temperature in the model was set by adjusting the atomic velocities. The time integration step in the molecular dynamics method was 1 fs.

The resulting particles were used as starting points for simulating the gradual heating and subsequent cooling of the particles. For particles of each size, simulations were conducted with constant heating rates from the monocrystalline state to temperatures significantly exceeding the melting point (from 600 to 2000 K for larger particles and generally up to 1800 K for relatively small particles) and reverse cooling from the molten state to 600 K (for crystallization simulation). The temperature change during heating and cooling was carried out at a constant rate by correspondingly adjusting the velocity magnitudes of all atoms in the model. It is known that when cooling melts at rates above $10^{13} – 10^{14}$ K/s, homogeneous crystallization does not have time to occur even in pure metals, resulting in metallic glasses [29; 30]. At the same time, as shown in studies [20 – 23] and will be demonstrated below, cooling rate of 10^{12} K/s is sufficient for crystallization to occur.

Results and discussion

The average potential energy of an atom was chosen as the primary characteristic of the state of the nanoparticle structure. Fig. 1 shows the dependence of the average atomic energy on temperature for particles with diameters of 8.0 and 2.5 nm during heating from the monocrystalline state and reverse cooling from the melt at different temperature change rates: $5 \cdot 10^{11}$, 10^{12} and $5 \cdot 10^{12}$ K/s. The sharp changes in the average atomic energy on the graphs apparently correspond to phase transitions: during the increase – melting, and during the decrease – crystallization. As is well known, the melting – crystallization phase transitions do not occur instantaneously; the crystal – liquid front moves at a finite speed, depending on the temperature, and usually ranges from several tens of meters per second [31; 32]. No stationary crystal – liquid front was observed; once formed, this front typically moved until the entire particle melted or crystallized. In light of the above, the phase transition temperatures were determined by the moment of their onset (indicated by arrows in Fig. 1).

Crystallization during gradual cooling from the melt occurred at a temperature significantly lower than the melting point. This substantial difference between the melting temperature (T_m) and the crystallization temperature (T_c) in nanoparticles is a well-known phenomenon in modeling [20; 22; 33]. As shown, the crystallization process is more sensitive to the rate of temperature change than melting: for all three rates, the onset of melting is roughly the same, while the crystallization

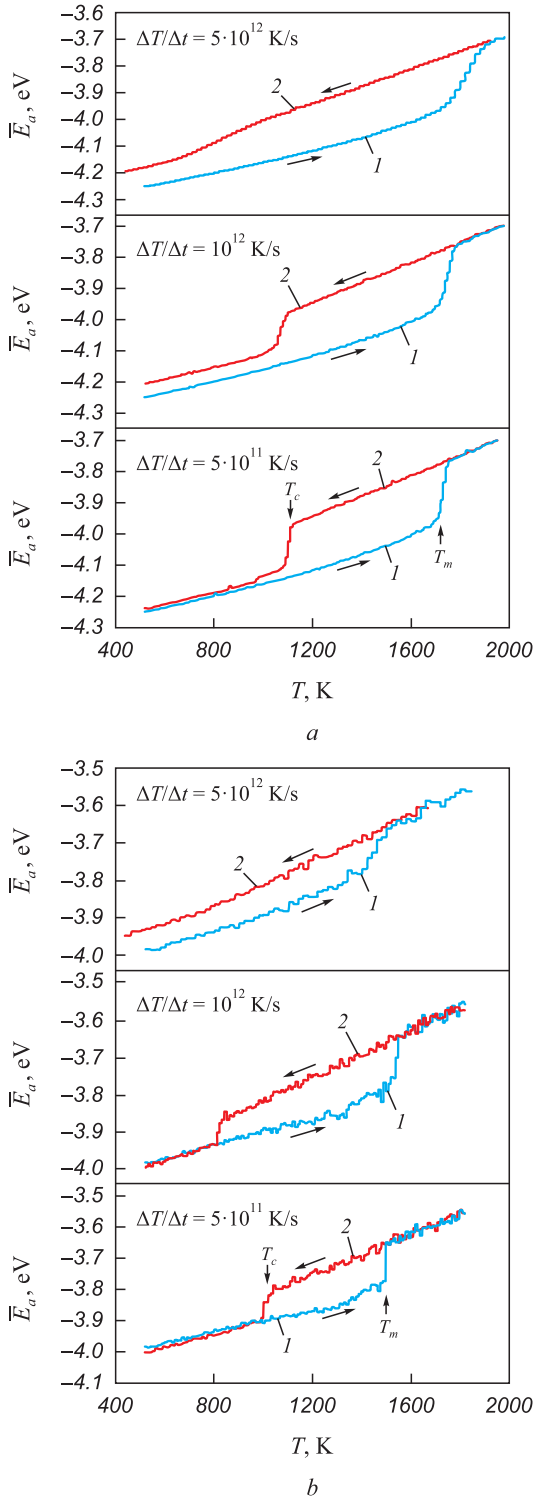

Fig. 1. Dependences of the average potential energy of an atom on temperature at different heating/cooling rates of austenite nanoparticles with a diameter of 8.0 (*a*) and 2.5 nm (*b*):
1 – heating of a single crystal particle;
2 – cooling of a particle from the molten state;
T_m – melting point; T_c – crystallization temperature

Рис. 1. Зависимости средней потенциальной энергии атома от температуры при разной скорости нагревания/охлаждения наночастиц аустенита диаметром 8,0 (*a*) и 2,5 нм (*b*):
1 – нагрев монокристаллической частицы;
2 – охлаждение частицы из расплавленного состояния;
T_m – температура плавления; T_c – температура кристаллизации

onset temperatures vary considerably. At a cooling rate of $5 \cdot 10^{12}$ K/s, crystallization only partially occurred for the 8.0 nm particle (as indicated by the relatively small drop in average atomic energy) and did not occur at all for the 2.5 nm particle (Fig, 1, *a*). As is well known, homogeneous crystallization involves two stages: nucleation of crystalline nuclei followed by their growth, i.e., the advancement of the crystallization front. These stages occur sequentially, and once stable nuclei are formed, the front moves at approximately the same speed as during melting, as evidenced by the similar slopes of the graphs during melting and crystallization in most cases.

It should be noted that for the 8.0 nm particle, after crystallization, the average atomic energy is higher than in the initial monocrystalline particle (Fig. 1, *a*, curve *2*), and the higher the cooling rate, the greater this difference. This is explained by the formation of a nanocrystalline structure after crystallization, characterized by higher average atomic energy values compared to the monocrystalline particle due to the presence of grain boundaries and other defects. The higher the cooling rate, the less time is spent on structural relaxation, and the higher the defect density in the cooled particle.

As the particle diameter decreased, the dependence of the average atomic energy on temperature underwent qualitative changes. Firstly, the energy difference between the crystalline and amorphous states was noticeably smaller compared to larger particles (Fig. 1, *b*). This is likely due to the relatively higher proportion of surface atoms in this case. Moreover, for smaller particles, the energy value fluctuations were higher, and the error in determining phase transition temperatures was greater, due to the relatively smaller number of atoms in them.

Another important change in the graphs with decreasing particle size was the decrease in melting and crystallization temperatures, as well as the stronger influence of the cooling rate on the crystallization temperature. This is obviously a consequence of the higher proportion of surface atoms as the particle diameter decreases. At a cooling rate of $5 \cdot 10^{12}$ K/s, crystallization did not occur at all for particles with diameters smaller than 3 nm, as evidenced by the absence of a downward energy jump corresponding to crystallization (e.g., Fig. 1, *b*, curve *2*).

Fig. 2 shows the atomic structure in a cross-section of particles with an 8.0 nm diameter, obtained using a crystalline phase visualizer. This visualizer determines the affiliation of each atom to a particular crystalline structure by analyzing the arrangement of neighboring atoms [34]. As seen in Fig. 2, with increasing cooling rate, grain sizes decrease, and the number of structural imperfections, including grain boundaries, increases. At a cooling rate of $5 \cdot 10^{11}$ K/s, judging by the very close positioning of curves *1* and *2* in Fig. 1, i.e., the slight dif-

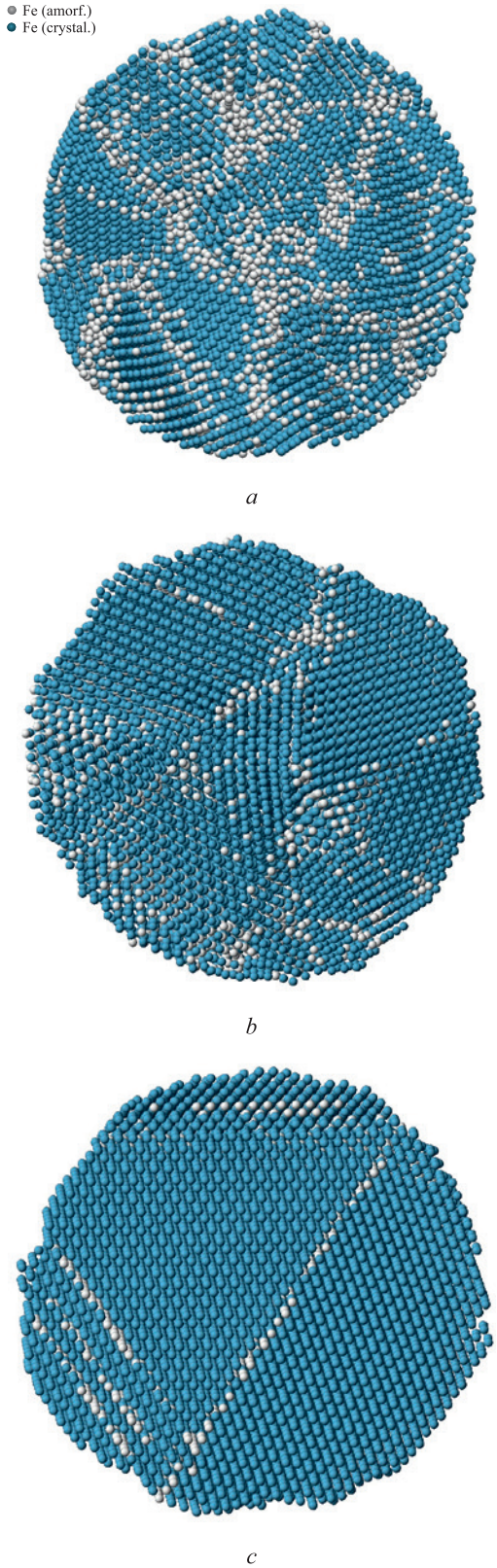

Fig. 2. Atomic structure of austenite particles with a diameter of 8.0 nm, free of carbon impurities, in a section obtained as a result of crystallization at a cooling rate of $5 \cdot 10^{12}$ (*a*), 10^{12} (*b*) and $5 \cdot 10^{11}$ K/s (*c*)

Рис. 2. Атомная структура частиц аустенита диаметром 8,0 нм, не содержащих примеси углерода, в срезе, полученная в результате кристаллизации при скорости охлаждения $5 \cdot 10^{12}$ (*a*), 10^{12} (*b*) и $5 \cdot 10^{11}$ К/с (*c*)

ference between the average energy of monocrystalline and crystallized particles, crystallization likely occurred often with the formation of low-energy grain boundaries (with a high density of coincident sites: special boundaries, twins).

To mathematically describe the influence of the free surface of nanoparticles on their melting temperature, a formula based on the assumption that the phase transition temperature change is proportional to the surface area-to-volume ratio of the particle is often used [35 – 37], i.e., for a spherical particle, this change should be proportional to $N^{-1/3}$ or d^{-1} (where N is the number of atoms in the particle; d is the particle diameter). In this study, the assumption for the crystallization temperature was used, with an added correction δ accounting for the finite thickness of the particle's surface layer:

$$T_c(d) = T_c^0\left(1 - \frac{\alpha_c}{d - \delta}\right), \qquad (1)$$

where T_c and T_c^0 are the crystallization temperatures of the particle and bulk material, respectively; α_c is a parameter that accounts for the extent of the particle surface's influence on its crystallization.

Formula (1) was used to construct an approximation curve for the dependence of the crystallization temperature of nanoparticles on their diameter (dashed lines in Fig. 3). As can be seen, for cooling rates of 10^{12} K/s and $5 \cdot 10^{11}$ K/s, the values obtained in the model (shown by markers in Fig. 4) closely match the approximation curves, confirming the leading role of the free surface not only in the melting process but also in the crystallization of nanoparticles. The parameter values for calculation by formula (1) were as follows (1): $T_c^0 = 1190$ K, $\alpha_c = 0.38$ K·nm, $\delta = 0.4$ nm for a cooling rate of $5 \cdot 10^{11}$ K/s

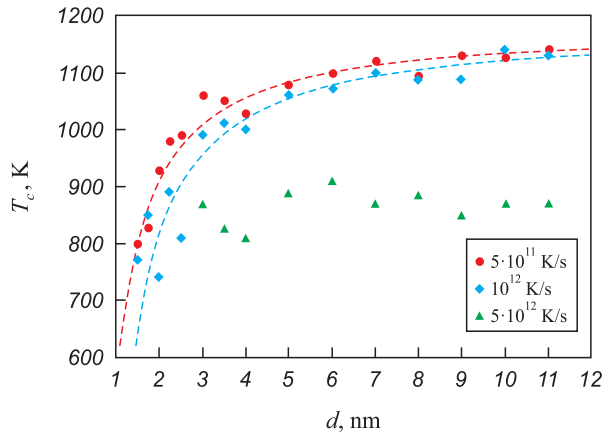

Fig. 3. Crystallization temperature of an austenite particle depending on its diameter at different melt cooling rates

Рис. 3. Температура кристаллизации частицы аустенита в зависимости от ее диаметра при разной скорости охлаждения расплава

and T_c^0 = 1190 K, α_c = 0.49 K·nm, δ = 0.4 nm for a cooling rate of 10^{12} K/s.

As shown in the dependencies in Fig. 3, the crystallization temperature increases as the cooling rate decreases. This fact confirms that the formation of nucleation sites is a probabilistic process requiring a relatively long time for the formation of stable nuclei. At a cooling rate of $5 \cdot 10^{12}$ K/s, particles with diameters smaller than 3 nm did not crystallize (triangular markers in Fig. 3). The error in determining the onset of crystallization at this rate was higher than at the other rates considered. Nevertheless, it is clear that at the highest of the rates considered, $5 \cdot 10^{12}$ K/s, crystallization occurs at lower temperatures than at lower rates.

The introduction of carbon impurity led to a decrease in the crystallization temperature. Fig. 4 shows the dependence of the crystallization temperature on particle diameter (Fig. 4, *a*) and carbon impurity concentration (Fig. 4, *b*). The following parameter values were obtained for calculation using formula (1): T_c^0 = 1155 K,

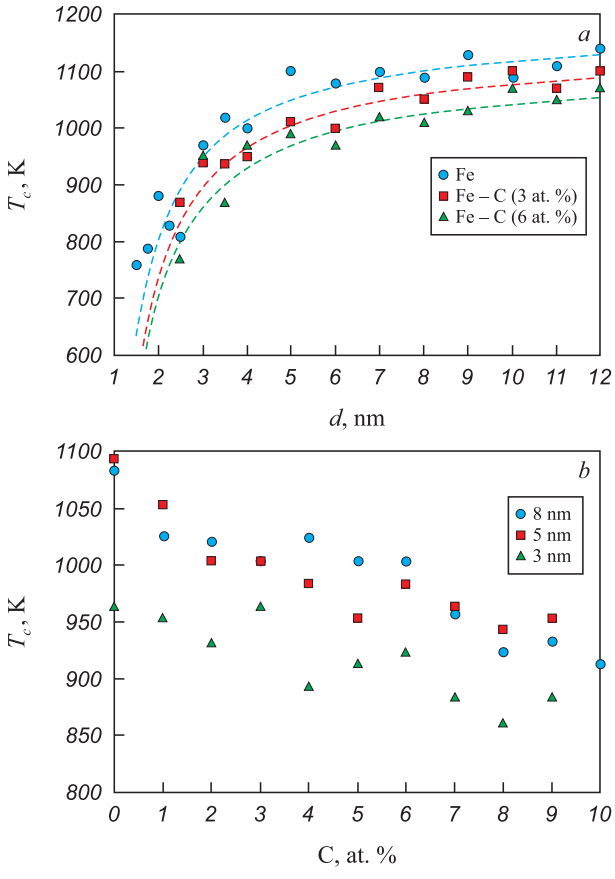

Fig. 4. Dependences of crystallization temperature of an austenite particle during cooling at a rate of 10^{12} K/s on the particle diameter at different concentrations of carbon impurity (*a*) and on carbon concentration at different particle sizes (*b*)

Рис. 4. Зависимости температуры кристаллизации частицы аустенита при охлаждении со скоростью 10^{12} К/с от диаметра частицы при разных концентрациях примеси углерода (*a*) и от концентрации углерода при разных размерах частиц (*b*)

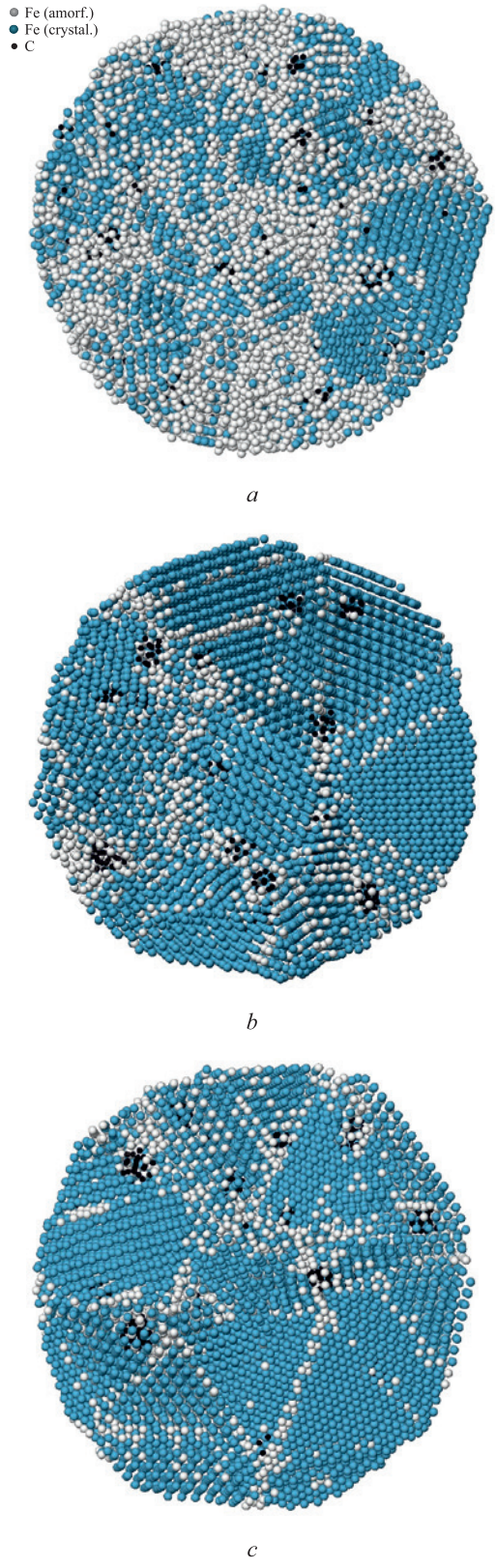

Fig. 5. Atomic structure of austenite particles with a diameter of 8.0 nm containing 3 at. % carbon, in the section obtained as a result of crystallization at a cooling rate of $5 \cdot 10^{12}$ (*a*), 10^{12} (*b*) and $5 \cdot 10^{11}$ K/s (*c*)

Рис. 5. Атомная структура частиц аустенита диаметром 8,0 нм, содержащих 3 ат. % углерода, в срезе, полученная в результате кристаллизации при скорости охлаждения $5 \cdot 10^{12}$ (*a*), 10^{12} (*b*) и $5 \cdot 10^{11}$ К/с (*c*)

α_c = 0.57 K·nm for a concentration of 3 at. %; T_c^0 = 1120 K, α_c = 0.59 K·nm for a concentration of 6 at. %. The δ value, which reflects the width of the surface layer, was found to be the same in all cases – 0.4 nm.

As the carbon concentration increased within the considered impurity atom concentration range, the crystallization temperature of the austenite particle decreased significantly: by nearly 200 K at a concentration of 10 at. % (Fig. 4, *b*). Carbon atoms, diffusing in the metal lattice, often formed clusters consisting of several carbon atoms (Fig. 5). These clusters distorted the emerging metal crystal lattice around them, hindering crystallization. Crystallization nuclei formed predominantly in the particle volume, followed by the intensive growth of crystals and the formation of a polycrystalline structure.

Fig. 5 shows the atomic structure of particles with a diameter of 8.0 nm, containing 3 at. % carbon, crystallized at different cooling rates. Comparing the structures shown in Fig. 2 for particles without carbon impurity, it is evident that the number of structural imperfections, grain boundaries, and other defects is significantly higher in the presence of carbon. The most notable difference was observed at the lowest cooling rate considered: $5 \cdot 10^{11}$ K/s. Without carbon impurity, the particle crystallized with a much lower defect density (Fig. 2, *c*) than in the presence of carbon (Fig. 5, *c*). In the latter case, the structure was almost indistinguishable from the structure obtained during cooling at a rate of 10^{12} K/s (Fig. 5, *b*). Carbon impurity atoms, especially clusters of them, predominantly settled at grain boundaries and triple junctions.

Conclusions

A study using molecular dynamics was conducted to investigate the struc-tural formation during the crystallization of austenite nanoparticles in the presence of carbon impurity. The effects of melt cooling rate, particle size, and carbon atom concentration on the crystallization process, resulting structural features, and crystallization onset temperature were examined. It was shown that the formation of a nanocrystalline structure in nanoparticles can be controlled by varying the cooling rate and introducing carbon impurity. In the model used, at a cooling rate above 10^{13} K/s, crystallization did not occur; at a rate below $5 \cdot 10^{12}$ K/s, the austenite particles crystallized, forming a nanocrystalline structure. Additionally, as the cooling rate decreased, the defect density in the final structure also decreased. At a cooling rate of $5 \cdot 10^{11}$ K/s or less, crystallization of carbon-free particles resulted in the formation of low-energy grain boundaries (with a high density of coincident sites: special boundaries, twins).

The crystallization temperature at a cooling rate below 10^{12} K/s is inverse-ly proportional to the particle diameter: as the particle size decreases, the proportion of the free surface increases, which reduces the probability of crystalline nuclei formation. Additionally, the crystallization temperature increases as the cooling rate decreases.

The introduction of carbon impurity led to a decrease in the crystallization temperature of nanoparticles: in the presence of 10 at. % carbon, the temperature decreased by approximately 200 K for particles of different sizes. Carbon atoms often formed clusters consisting of several atoms. These clusters distorted the forming metal crystal lattice around them, hindering crystallization. In the presence of carbon impurity, the final structure of the crystallized particles contained a higher density of grain boundaries and other defects. Carbon atoms, especially in clusters, predominantly settled at grain boundaries and triple junctions.

References / Список литературы

1. Humbert C., Noblet T., Dalstein L., Busson B., Barbillon G. Sum-frequency generation spectroscopy of plasmonic nanomaterials: A review. *Materials*. 2019;12(5):836. https://doi.org/10.3390/ma12050836
2. Mantri Y., Jokerst J.V. Engineering plasmonic nanoparticles for enhanced photoacoustic imaging. *ACS Nano*. 2020;14(8): 9408–9422. https://doi.org/10.1021/acsnano.0c05215
3. Jain T.K., Morales M.A., Sahoo S.K., Leslie-Pelecky D.L., Labhasetwar V. Iron oxide nanoparticles for sustained delivery of anticancer agents. *Molecular Pharmaceutics*. 2005; 2(3):194–205. https://doi.org/10.1021/mp0500014
4. Shim S.Y., Lim D.K., Nam J.M. Ultrasensitive optical biodiagnostic methods using metallic nanoparticles. *Nanomedicine*. 2008;3(2):215–232. https://doi.org/10.2217/17435889.3.2.215
5. Kodama K., Nagai T., Kuwaki A., Jinnouchi R., Morimoto Y. Challenges in applying highly active Pt-based nanostructured catalysts for oxygen reduction reactions to fuel cell vehicles. *Nature Nanotechnology*. 2021;16:140–147. https://doi.org/10.1038/s41565-020-00824-w
6. Mitchell S., Qin R., Zheng N., Perez-Ramirez J. Nanoscale engineering of catalytic materials for sustainable technologies. *Nature Nanotechnology*. 2021;16:129–139. https://doi.org/10.1038/s41565-020-00799-8
7. Wagener P., Jakobi J., Rehbock C., Chakravadhanula V.S.K., Thede C., Wiedwald U., Bartsch M., Kienleand L., Barcikowski S. Solvent-surface interactions control the phase structure in laser-generated iron-gold core-shell nanoparticles. *Scientific Reports*. 2016;6:23352. https://doi.org/10.1038/srep23352
8. Ziefub A.R., Reichenberger S., Rehbock C., Chakraborty I., Gharib M., Parak W.J., Barcikowski S. Laser fragmentation of colloidal gold nanoparticles with high-intensity nanosecond pulses is driven by a single-step fragmentation mechanism with a defined educt particle-size threshold. *The Journal of Physical Chemistry C*. 2018;122(38):22125–22136. https://doi.org/10.1021/acs.jpcc.8b04374
9. Amikura K., Kimura T., Hamada M., Yokoyama N., Miyazaki J., Yamada Y. Copper oxide particles produced by laser ablation in water. *Applied Surface Science*. 2008;254(21): 6976–6982. https://doi.org/10.1016/j.apsusc.2008.05.091

10. Barcikowski S., Compagnini G. Advanced nanoparticle generation and excitation by lasers in liquids. *Physical Chemistry Chemical Physics*. 2013;15(9):3022–3026. https://doi.org/10.1039/C2CP90132C
11. Liang S.-X., Zhang L.-C., Reichenberger S., Barcikowski S. Design and perspective of amorphous metal nanoparticles from laser synthesis and processing. *Physical Chemistry Chemical Physics*. 2021;23(19):11121–11154. https://doi.org/10.1039/D1CP00701G
12. Sun J., Sinha S.K., Khammari A., Picher M., Terrones M., Banhart F. The amorphization of metal nanoparticles in graphitic shells under laser pulses. *Carbon*. 2020;161:495–501. https://doi.org/10.1016/j.carbon.2020.01.067
13. He D.S., Huang Y., Myers B.D., Isheim D., Fan X., Xia G.-J., Deng Y., Xie L., Han S., Qiu Y., Wang Y.-G., Luan J., Jiao Z., Huang L., Dravid V.P., He J. Single-element amorphous palladium nanoparticles formed via phase separation. *Nano Research*. 2022;15:5575–5580. https://doi.org/10.1007/s12274-022-4173-1
14. Qian Y., Silva A., Yu E., Anderson C.L., Liu Y., Theis W., Ercius P., Xu T. Crystallization of nanoparticles induced by precipitation of trace polymeric additives. *Nature Communications*. 2021;12(1):2767. https://doi.org/10.1038/s41467-021-22950-2
15. Pei Y., Zhou G., Luan N., Zong B., Qiao M., Tao F. Synthesis and catalysis of chemically reduced metal-metalloid amorphous alloys. *Chemical Society Reviews*. 2012;41(24): 8140–8162. https://doi.org/10.1039/c2cs35182j
16. Jia Z., Wang Q., Sun L., Wang Q., Zhang L.C., Wu G., Luan J.H., Jiao Z.B., Wang A., Liang S.X., Gu M., Lu J. Metallic glass catalysts: attractive in situ self-reconstructed hierarchical gradient structure of metallic glass for high efficiency and remarkable stability in catalytic performance. *Advanced Functional Materials*. 2019;29(19): 1970131. https://doi.org/10.1002/adfm.201970131
17. Chen Q., Yan Z., Guo L., Zhang H., Zhang L.-C., Wang W. Role of maze like structure and Y_2O_3 on Al-based amorphous ribbon surface in MO solution degradation. *Journal of Molecular Liquids*. 2020;318:114318. https://doi.org/10.1016/j.molliq.2020.114318
18. Kumar K.S., Van Swygenhoven H., Suresh S. Mechanical behavior of nanocrystalline metals and alloys. *Acta Materialia*. 2003;51(19):5743–5774. https://doi.org/10.1016/j.actamat.2003.08.032
19. Meyers M.A., Mishra A., Benson D.J. Mechanical properties of nanocrystalline materials. *Progress in Materials Science*. 2006;51(4):427–556. https://doi.org/10.1016/j.pmatsci.2005.08.003
20. Nguyen T.D., Nguyen C.C., Tran V.H. Molecular dynamics study of microscopic structures, phase transitions and dynamic crystallization in Ni nanoparticles. *RSC Advances*. 2017;7(41):25406–25413. https://doi.org/10.1039/C6RA27841H
21. Trang G.T.T., Kien P.H., Hung P.K., Ha N.T.T. Molecular dynamics simulation of microstructure and atom-level mechanism of crystallization pathway in iron nanoparticle. *Journal of Physics: Conference Series*. 2020;1506:012020. https://doi.org/10.1088/1742-6596/1506/1/012020
22. Poletaev G.M., Gafner Y.Y., Gafner S.L. Molecular dynamics study of melting, crystallization and devitrification of nickel nanoparticles. *Letters on Materials*. 2023;13(4):298–303. https://doi.org/10.22226/2410-3535-2023-4-298-303
23. Poletaev G.M., Bebikhov Y.V., Semenov A.S. Molecular dynamics study of the formation of the nanocrystalline structure in nickel nanoparticles during rapid cooling from the melt. *Materials Chemistry and Physics*. 2023;309:128358. https://doi.org/10.1016/j.matchemphys.2023.128358
24. Lau T.T., Forst C.J., Lin X., Gale J.D., Yip S., Van Vliet K.J. Many-body potential for point defect clusters in Fe–C alloys. *Physical Review Letters*. 2007;98(21):215501. https://doi.org/10.1103/PhysRevLett.98.215501
25. Oila A., Bull S.J. Atomistic simulation of Fe-C austenite. *Computational Materials Science*. 2009;45(2):235–239. https://doi.org/10.1016/j.commatsci.2008.09.013
26. Lv B., Chen C., Zhang F., Poletaev G.M., Rakitin R.Y. Potentials for describing interatomic interactions in γFe–Mn–C–N system. *Metals*. 2022;12(6):982. https://doi.org/10.3390/met12060982
27. Poletaev G., Gafner Y., Gafner S., Bebikhov Y., Semenov A. Molecular dynamics study of the devitrification of amorphous copper nanoparticles in vacuum and in a silver shell. *Metals*. 2023;13(10):1664. https://doi.org/10.3390/met13101664
28. Gafner Y., Gafner S., Redel L., Poletaev G. Estimation of the structure of binary Ag-Cu nanoparticles during their crystallization by computer simulation. *Journal of Nanoparticle Research*. 2023;25:205. https://doi.org/10.1007/s11051-023-05850-y
29. Liang S.–X., Zhang L.–C., Reichenberger S., Barcikowski S. Design and perspective of amorphous metal nanoparticles from laser synthesis and processing. *Physical Chemistry Chemical Physics*. 2021;23(19):11121–11154. https://doi.org/10.1039/D1CP00701G
30. Zhong L., Wang J., Sheng H., Zhang Z., Mao S.X. Formation of monatomic metallic glasses through ultrafast liquid quenching. *Nature*. 2014;512:177–180. https://doi.org/10.1038/nature13617
31. Chan W.–L., Averback R.S., Cahill D.G., Ashkenazy Y. Solidification velocities in deeply undercooled silver. *Physical Review Letters*. 2009;102(9):095701. https://doi.org/10.1103/PhysRevLett.102.095701
32. Zhang H.Y., Liu F., Yang Y., Sun D.Y. The molecular dynamics study of vacancy formation during solidification of pure metals. *Scientific Reports*. 2017;7:10241. https://doi.org/10.1038/s41598-017-10662-x
33. Qi Y., Cagin T., Johnson W.L., Goddard III W.A. Melting and crystallization in Ni nanoclusters: the mesoscale regime. *The Journal of Chemical Physics*. 2001;115(1):385–394. https://doi.org/10.1063/1.1373664
34. Tsuzuki H., Branicio P.S., Rino J.P. Structural characterization of deformed crystals by analysis of common atomic neighborhood. *Computer Physics Communications*. 2007; 177(6):518–523. https://doi.org/10.1016/j.cpc.2007.05.018
35. Xiong S., Qi W., Cheng Y., Huang B, Wang M., Li Y. Universal relation for size dependent thermodynamic properties of metallic nanoparticles. *Physical Chemistry Chemical Physics*. 2011;13(22):10652–10660. https://doi.org/10.1039/C0CP90161J
36. Nanda K.K. Liquid-drop model for the surface energy of nanoparticles. *Physics Letters A*. 2012;376(19):1647–1649. https://doi.org/10.1016/j.physleta.2012.03.055
37. Safaei A., Attarian Shandiz M., Sanjabi S., Barber Z.H. Modeling the melting temperature of nanoparticles by an analytical approach. *The Journal of Physical Chemistry C*. 2008;112(1):99–105. https://doi.org/10.1021/jp0744681

Information about the Authors

***Irina V. Zorya*,** *Dr. Sci. (Phys.-Math.), Prof., Head of the Chair of Heat-Gas-Water Supply, Water Disposal and Ventilation,* Siberian State Industrial University
ORCID: 0000-0001-5748-813X
E-mail: zorya.i@mail.ru

***Gennadii M. Poletaev*,** *Dr. Sci. (Phys.-Math.), Prof., Head of the Chair of Advanced Mathematics,* Polzunov Altai State Technical University; *Prof.,* Katanov Khakassian State University
ORCID: 0000-0002-5252-2455
E-mail: gmpoletaev@mail.ru

***Yurii V. Bebikhov*,** *Cand. Sci. (Phys.-Math.), Assist. Prof.,* Mirny Polytechnic Institute (branch) of North-Eastern Federal University
ORCID: 0000-0002-8366-4819
E-mail: bebikhov.yura@mail.ru

***Aleksandr S. Semenov*,** *Dr. Sci. (Phys.-Math.), Director,* Mirny Polytechnic Institute (branch) of North-Eastern Federal University
ORCID: 0000-0001-9940-3915
E-mail: as.semenov@s-vfu.ru

Сведения об авторах

***Ирина Васильевна Зоря*,** *д.ф.-м.н., профессор, заведующий кафедрой теплогазоводоснабжения, водоотведения и вентиляции,* Сибирский государственный индустриальный университет
ORCID: 0000-0001-5748-813X
E-mail: zorya.i@mail.ru

***Геннадий Михайлович Полетаев*,** *д.ф.-м.н., профессор, заведующий кафедрой высшей математики,* Алтайский государственный технический университет им. И.И. Ползунова; *профессор,* Хакасский государственный университет им. Н.Ф. Катанова
ORCID: 0000-0002-5252-2455
E-mail: gmpoletaev@mail.ru

***Юрий Владимирович Бебихов*,** *к.ф.-м.н., доцент,* Политехнический институт Северо-Восточного федерального университета им. М. К. Аммосова
ORCID: 0000-0002-8366-4819
E-mail: bebikhov.yura@mail.ru

***Александр Сергеевич Семенов*,** *д.ф.-м.н., директор,* Политехнический институт Северо-Восточного федерального университета им. М. К. Аммосова
ORCID: 0000-0001-9940-3915
E-mail: as.semenov@s-vfu.ru

Contribution of the Authors

I. V. Zorya – problem statement, literary analysis, processing of results, writing the main text.
G. M. Poletaev – problem statement, development of a computer model, literary analysis, processing of results, editing the article final version.
Yu. V. Bebikhov – performing calculations and obtaining results, creating drawings and graphs.
A. S. Semenov – performing calculations and obtaining results, creating drawings and graphs.

Вклад авторов

И. В. Зоря – постановка задачи, анализ литературных источников, обработка результатов, написание основного текста статьи.
Г. М. Полетаев – постановка задачи, разработка компьютерной модели, анализ литературных источников, обработка результатов, редактирование финальной версии статьи.
Ю. В. Бебихов – проведение расчетов и получение результатов, создание рисунков и графиков для статьи.
А. С. Семенов – проведение расчетов и получение результатов, создание рисунков и графиков для статьи.

Поступила в редакцию 18.03.2024
После доработки 05.04.2024
Принята к публикации 10.04.2024

Received 18.03.2024
Revised 05.04.2024
Accepted 10.04.2024